Applied Nanoscience (2020) 10:4591–4602
https://doi.org/10.1007/s13204-020-01313-1

ORIGINAL ARTICLE

Composites based on zirconium dioxide and zirconium hydrophosphate containing graphene-like additions for removal of U(VI) compounds from water

O. V. Perlova[1] · Yu. S. Dzyazko[2] · A. V. Palchik[2] · I. S. Ivanova[1] · N. O. Perlova[1] · M. O. Danilov[2] · I. A. Rusetskii[2] · G. Ya. Kolbasov[2] · A. G. Dzyazko[3]

Received: 25 November 2019 / Accepted: 18 February 2020 / Published online: 12 March 2020

Abstract
The composites based on hydrated zirconium dioxide and zirconium hydrophosphate have been obtained. The materials contained 0.5–7% of graphene-like additions, which were obtained by chemical treatment of multiwalled carbon nanotubes (8–15 layers). The composites as well as their constituents were investigated with the XRD, FTIR, TEM, and porometric methods. When the content of carbon material is 2%, large granules (0.3–0.35 mm) are formed. GO was found to increase specific surface area of zirconium hydrophosphate and reduces it in the case of zirconium dioxide. Despite the small amount of GO additions, these composites show a growth of total sorption capacity of 12–14% in alkaline media. Sorption of cationic complexes of U(VI) under batch conditions was investigated. The composite based on zirconium hydrophosphate allows us to remove U(VI) from water practically completely in the presence of hardness ions; the highest regeneration degree is also achieved. Sorption kinetics is described by the model of pseudo-second order. The Dubinin–Raduchkevich model was applied to adsorption isotherms. As found, the mechanism of sorption is ion exchange that is accompanied by additional interaction of sorbed ions with functional groups.

Keywords Uranium · Zirconium phosphate · Zirconium oxide · Graphene oxide · Composite · Sorption

Introduction

Soluble uranium (VI) compounds occur in sources of water supply (ground water, lakes, and rivers) as a results of leaching from natural deposits, release in mill tailings, emissions from nuclear power plants, combustion of coal or other fuels, and even due to use of the phosphate fertilizers (Alirezazadeh and Garshasbi 2003; Hoover et al. 2017; Orloff et al. 2004). Maximum permissible concentration for soluble compounds of uranium is 0.015 mg dm^{-3}. Lower values are also recommended (Brine 2010), since this metal is not only radioactive, but also toxic.

To remove small amounts of U(VI) from water, adsorption methods, particularly ion exchange, are preferable (Awwad 2018; Everett 1998). As opposite to other techniques, such as chemical (Ling et al. 2015), photocatalytic (Liu et al. 2018), or biological (Gilson et al. 2015) reduction of U(VI) to U(IV) (formation of insoluble UO_2), adsorption method leads to no formation of finely dispersed substance, and provides the most complete uranium recovery.

A number of commercial polymer ion exchangers are used for uranium sorption, namely ion-exchange resins (Gu et al. 2004; Wen et al. 2019; Outokesh et al. 2016) and fibers (Perlova et al. 2019; Sazonova et al. 2017). Improvement of selectivity towards U(VI) is achieved by additional functionalization with organic substances (Dragan et al. 2004; Metilda et al. 2005) or nanoparticles of ion exchangers (Dzyazko et al. 2017; Perlova et al. 2017, 2018). However, radionuclides provoke the degradation of polymer ion exchangers, and the products of polymer destruction form complexes with radioactive ions impeding their removal

✉ I. S. Ivanova
inna_ivanova_2512@ukr.net

[1] Odesa I.I. Mechnikov National University, Dvoryanska str. 2, Odesa 65082, Ukraine

[2] V.I. Vernadskii Institute of General and Inorganic Chemistry of the NAS of Ukraine, Palladin ave. 32/34, Kyiv 03142, Ukraine

[3] Taras Shevchenko National University of Kyiv, Volodymyrska str. 64/13, Kyiv 01601, Ukraine

from water (Kao et al. 2016; Leybros et al. 2010; Loon and Hummel 1999). Moreover, polymer ion exchangers are fouled with organic species (Gönder et al. 2006) or inorganic colloidal particles, which are formed during equipment corrosion (Zvezdov and Ishigure 2003).

Inorganic ion exchangers, such as hydrated oxides or hydrophosphate of multivalent metals, look attractive for U(VI) sorption (Ali 2018; Amphlett 1964; Liu et al. 2016; Reinoso-Maset and Ly 2016; Wang et al. 2016; Zakutevskyy et al. 2012), since they are stable against ionizing radiation and fouling. They possess higher selectivity towards U(VI) compounds, since sorption is accompanied by the complex formation with phosphate (Drot et al. 1998; Almazan-Torres et al. 2008; Ordoñez-Regil et al. 2003) or hydroxide (Pan et al. 2017; Um et al. 2008) functional groups. Similar effect has been also found for sorption of d metals on phosphates (Dzyazko et al. 2013).

However, the inorganic materials are very sensitive to the solution acidity. Dissociation of hydrophosphate functional groups becomes sufficient at pH > 2; dissociation of—OH groups dominates in alkaline media (Amphlett 1964). Moreover, speciation of U(VI) ions is strongly dependent on pH and salt background (Cornelis et al. 2005): U(VI) ions are in cationic forms in sulphuric or nitric acid; anionic species dominate in carbonate or chloride media. It should be also noted that sorption of UO_2^{2+} on both natural (Bachmaf and Merkel 2011) and synthetic (Criscenti and Sverjensky 1999) inorganic materials is depressed by Cl^- ions, which are usually contained in water.

At the same time, graphene oxide (GO) can be recommended as a modifier of inorganic materials for improvement their sorption properties, since it is characterized by high adsorption capacity caused by the developed surface, where carboxyl and phenolic functional groups are located (Dreyer et al. 2010). This two-dimensional carbon nanomaterial was applied to modifying hydrated zirconium dioxide, HZD (Dzyazko et al. 2018; Seredych and Bandosz 2010,2011), or zirconium hydrophosphate, ZHP (Pourbeyram, 2016). GO is an effective adsorbent of U(VI) cationic species (Yang et al. 2018). However, the GO production from graphite involves a number of aggressive reagents ($KMnO_4$, HNO_3, and so on) (Dreyer et al. 2010). Moreover, the synthesis process is dangerous from the point of view of safety. More safe and eco-friendly synthesis can be performed using multiwalled carbon nanotubed (MWCNTs); multilayered GO-like materials (GO_{lm}), namely GO nanoribbons, are obtained by chemical or electrochemical methods (Danilov et al. 2016a). It is expected that this modifier will improve adsorption properties of inorganic ion exchangers towards U(VI) ions. The necessary requirements for ion exchanger are coarse mechanically durable granules: this would give a possibility to use the sorbent as a filler of sorption columns.

The aim of this work is to establish the effect of GO_{lm}, which was obtained from MWCNTs, on the grade of the composites based on HZD and ZHP, as well as its influence on sorption of U(VI) ions on these materials. The tasks of the work also involve characterization of the composite materials.

Experimental

Materials

Multiwalled carbon nanotubes (MWCNTs) of standard characteristics were the initial material for the GO_{lm} synthesis. They have been purchased from the "TM Spetzmash" LTD. Their outer diameter was 10–30 nm, the bulk density was 25–30 g dm^{-3}, the wall amount was 8–15, and the specific surface area was 130 m^2g^{-1}.

Such reagents as $ZrOCl_2 \cdot 8H_2O$, NH_4OH, H_3PO_4, $K_2Cr_2O_7$, H_2SO_4, HCl, HNO_3, and NaOH were purchased from the Cherkassy KhimProm LTD (Ukraine). The $UO_2Ac_2 \cdot 2H_2O$ salt was produced by Chemapol, Czech Republic.

Synthesis of GO_{lm} and composites based on HZD and ZHP

Graphene-like carbon material, which consists of several grapheme sheets (8–15 according to the numbers of MWCNTs' layers), was synthesized according to the method described in (Danilov et al. 2016a). In general, the methods that allow one to open carbon nanotubes are summarized in (Danilov et al. 2016b). Briefly, 1 g of MWCNTs was added to 30 cm^3 of H_2SO_4 solution (98%), the suspension was stirred during 1 h. After this, 10 g of $K_2Cr_2O_7$ was added, and the mixture was stirred during 72 h. Furthermore, the dispersion was filtered and washed subsequently with a HCl solution and distilled water. Then, the obtained powder was dispersed in water (2.8 mg cm^{-3}).

Sol of insoluble zirconium hydroxocomplexes was obtained similarly to (Dzyazko et al. 2014; Dzyaz'ko et al. 2006) by means of gradual adding of a NH_4OH solution to a 1 M $ZrOCl_2$ solution under intensive stirring at 80 °C. Then, sol was boiled for 48 h and stored under room temperature. Relatively to anhydrous zirconium oxide, 100 cm^3 of sol contained 12.3 g ZrO_2.

Sol (100 cm^3) and GO_{lm} suspension (22.5, 45, 90, 135, 220, and 307 cm^3) were mixed und activated with ultrasound for 5 min at 30 kHz using a Bandeline bath (Bandeline). Then, the GO_{lm}-containing suspension was added to saturated NaOH solution, the beads were washed subsequently with a 1 M NH_4OH solution and deionized water. Pure HZD hydrogel was obtained from sol by the same manner. A part of hydrogels,

which were obtained by precipitation from sol or GO_{lm} suspension in sol, was washed repeatedly with deionized water down to pH 7 of the effluent. Then, hydrogels were dried under room temperature down to constant mass.

Other part of hydrogels (pure and GO_{lm}-containing HZD) was boiled in a 1 M H_3PO_4 for 1 h, washed with deionized water up to pH 7, and dried under room temperature. The samples HZD-GO_{lm} and ZHP-GO were obtained by this manner. The samples contained 0.5, 1, 2, 3, 5, and 7 mass % of GO_{lm} relatively anhydrous ZrO_2.

Dry sorbents were sieved, and fractions of 0.8–1, 0.5–0.8, 0.25–0.5, 0.2–0.25, 0.1–0.2, and < 0.1 mm were taken and weighted. Before the investigations, the samples of HZD and HZD-GO_{lm} were regenerated electrochemically at 90 V using a three-compartment cell supplied with ion-exchange membranes. This was necessary to remove NH_4^+ ions from the solids. The cell construction and equipment are described in (Dzyazko et al. 2019).

Characterization of samples

In this work, the samples based on HZD and ZHP composites containing 2% of GO_{lm} were in a focus of attention, since they are characterized by optimal functional properties. Pure inorganic sorbents were also considered for comparison.

FTIR spectra were recorded using a Spectrum BX FT-IR spectrometer (PerkinElmer Instruments, USA). Before the measurements, the samples were grinded and compressed with KBr, which was preliminarily grinded and dried at 135 °C. The mixture was compressed at 10 bars.

The XRD patterns of the grinded samples applied to glass substrates were obtained by means of a DRON-3 spectrometer (Burevestnik, RF) supplied with tungsten cathode, copper anode, and nickel filter. The sample was inserted into a quartz capillary, a diameter of which was 0.5 mm. The measurements were within the interval of $2\theta = 0–90°$, the step was 0.01°. The current was 4 A.

Visualization of the sample structure was carried out using a JEOL JEM 1230 transmission electron microscope (Jeol, Japan). Preliminarily, the samples were grinded and fixed on copper substrates as thin films. Accelerating voltage was 120 kV.

Before sieving, the granule size of some sorbents was estimated using a Crystal-45 optical microscope (Konus, USA). 300 particles for each sample were analyzed. The particle-size distributions were plotted as dependencies of particle fraction (W) on grain diameter. The W value was calculated via:

$$W_i = \frac{q_i}{\sum_{i=1} q_i}. \quad (1)$$

The method of adsorption–desorption of nitrogen was used for porosimetric measurement. The Autosorb Nova-6B device (Quantochrome Instruments, USA) was applied to the investigations.

Potentiometric titration was carried out by means the solid addition method (Somasekhara Reddy et al. 2012) using a 0.1 M KNO_3 solution. The solution pH was regulated with HCl and NaOH solutions. The solution pH was measured with I-160MI pH meter (Izmeritelnaya technika, Republic of Belarus).

Adsorption testing

All adsorption experiments that are described in this and next subsections were carried out under batch conditions at 25 °C. The samples of different composition were used for the preliminary test. 50 dm^3 of a 0.1 M KOH solution was added to 2 g of sorbent. After 48 h, the alkali solution and solid were separated, and the sorbent was washed with deionized water down to pH 7 of the effluent. Then, the sample was treated three times with a 0.1 M HNO_3 solution to provide the most complete regeneration. K^+ ions in the effluent were analyzed with a PFM-U4.2 flame photometer (Analitpribor, Republic of Belarus).

Uranium adsorption and sorbent regeneration

The materials containing 2% of GO_{lm}, as well as pure HZD and ZHP were researched. The sorbent mass was 0.1 g; the solution volume was 50 cm^3. For the preparation of U(VI)-containing solution, HNO_3 was added to tap water. Water contained initially 1.2 mmol dm^{-3} Ca^{2+} and 0.5 mmol dm^{-3} Mg^{2+}; the resulting acid concentration was 0.02 mol dm^{-3}. Uranyl acetate was dissolved in this solution; nitric acid provided cationic forms of U(VI). The solution pH was regulated by adding NaOH solution. The U(VI) content was determined using a Shimadzu UV-mini1240 spectrophotometer (Shimadzu, Japan) at 670 nm (Kadam et al. 1981). Preliminarily, U(VI) was transformed into a complex with Arsenazo III. The initial (C_0) and equilibrium (C) concentration was obtained by this manner. The degree of uranium removal (S) was calculated as $\frac{C_0-C}{C_0} \times 100\%$; capacity ($A$) was determined as $\frac{V(C_0-C)}{m}$; where V is the solution volume and m is the sorbent mass.

To investigate adsorption rate, the solution containing 25 mg dm^{-3} of U(VI) was used, and the initial pH was seven. When sorbent was added, the flask content was intensively stirred with a Water Bath Shaker Type 357 system (Elpan, Poland). After the predetermined time, the solution probe (1 cm^3) was taken and analyzed later. The effect of pH on sorption was investigated using the solution containing 25 mg dm^{-3} of U(VI); the sorption time was 24 h. When sorption isotherms were obtained, the initial solution

concentration of U(VI) was 5–25 mg dm^{-3}, the pH was seven, and the adsorption time was 120 h.

Regeneration of loaded samples was carried out by means of deionized water or 0.1 M $NaHCO_3$ or HNO_3 solutions. The sorbent mass was 0.1 g. The volume of the solution for regeneration was 50 cm^3. The regeneration degree was calculated as $R_d = \frac{C_d}{C_0 - C} \times 100\%$, where C_d is the effluent concentration.

Results and discussion

Effect of GO_{lm} on grading sorbents

HZD and ZHP samples are coarse white grains; their shape is close to spherical. The granules of the composites containing GO_{lm} are black. GO_{lm} affect the grain size of the sorbents, as shown in Fig. 1a. The figure illustrates the dependence of the average granule diameter of the heaviest (dominating) fraction on the content of this carbon material. Increasing in the GO_{lm} amount reduces a size of the granules, which are formed during synthesis.

Figure 1b illustrates detailed granule size distribution for both pure inorganic sorbents and their composites containing 2% of GO_{lm}. As seen, ZHP forms larger granules than HZD due to cross-linkage of hydrogel with Zr–O–P–O–Zr bonds. Addition of GO_{lm} to both ZHP and HZD results in a decrease of the granule size of dominating fraction in ≈2 times.

Visualization of primary particles

TEM image of MWCNTs is given in Fig. 2a. Both straight and stranded nanotubes are seen; the diameter of the straight ones is about 30 nm. Chemical treatment causes partial expansion of the nanotubes: GO_{lm} sheets are seen (Fig. 2b). However, some of undisclosed nanotubes are present in the bulk of the carbon material.

Nanoparticles, a size of which is 6 nm, dominates in sol of insoluble zirconium hydroxocomplexes (Dzyazko et al. 2014). During precipitation, the nanoparticles are merged due to the formation of Zr–O–Zr bonds. As a result, larger strongly aggregated particles (≈20–50 nm) are formed (Fig. 2c). Their shape is close to spherical. The particles of irregular shape are formed during ZHP deposition (Fig. 2d). In general, they are larger than 100 nm. These formations are evidently splices of smaller particles; coalescence is caused by Zr–O–P–O–Zr bonds.

Addition of GO_{lm} causes loosening of inorganic nanoparticles (Fig. 3a, b) due to their adsorption on carbon sheets. GO_{lm} forms more compact coating in the surface of ZHP, the primary particles of which cannot be recognized as opposed to HZD. High-resolution image of coated ZHP particles is typical for graphene materials (Fig. 3c). The stripes correspond to the expended graphite nanosheets.

XRD and FTIR spectroscopy

XRD patterns of MWCNTs are shown in Fig. 4. The (002) peak corresponds to $2\theta = 26.02°$; it corresponds to the reflex from the interplanar distance between graphite layers. The position of this reflex depends on the MWCNTs thickness (Futaba et al. 2011; Zhao et al. 2015). The reflex is not narrow, since the wall numbers are within the interval of 8–15. The diffuse symmetric reflex about $2\theta = 21°$ is due to SiO_2 of a capillary.

In the case of GO_{lm}, the reflex at $2\theta = 26.02°$ disappears; the peak attributed to SiO_2 shows a diffuse shoulder from the side of smaller angles. This shoulder is related to GO_{lm}. Regarding GO, the narrow reflex at 11.4° has to be

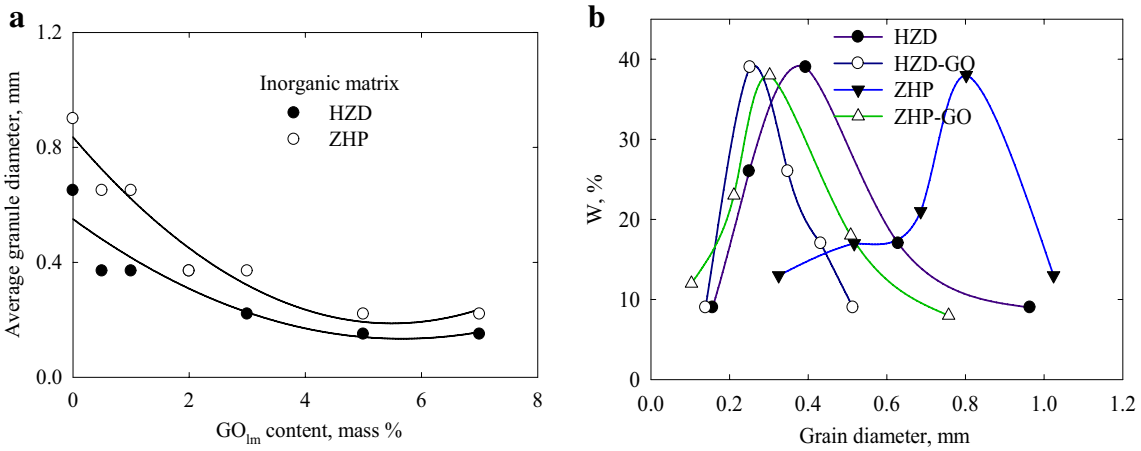

Fig. 1 Average granule diameter of the dominating fraction of sorbents as a function of GO_{lm} content (**a**), grain size distribution of pure inorganic sorbents and their composites containing 2% of GO_{lm} (**b**).

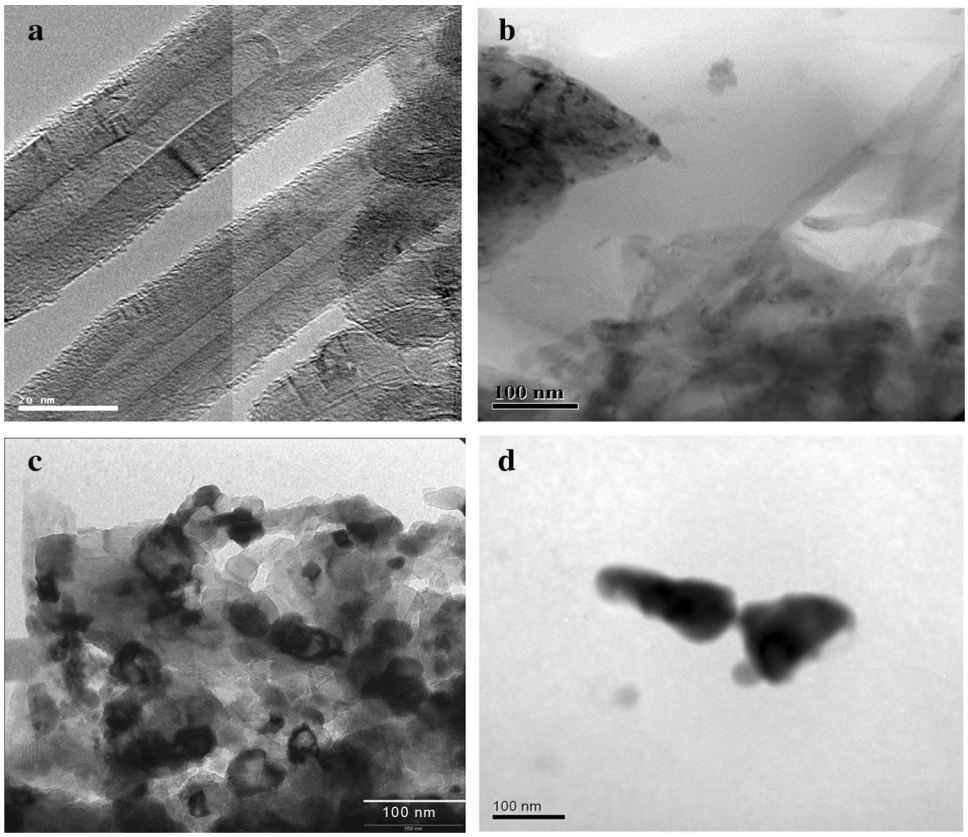

Fig. 2 TEM images of MWCNTs (**a**), GO_{lm} (**b**), HZD (**c**), and ZHP (**d**)

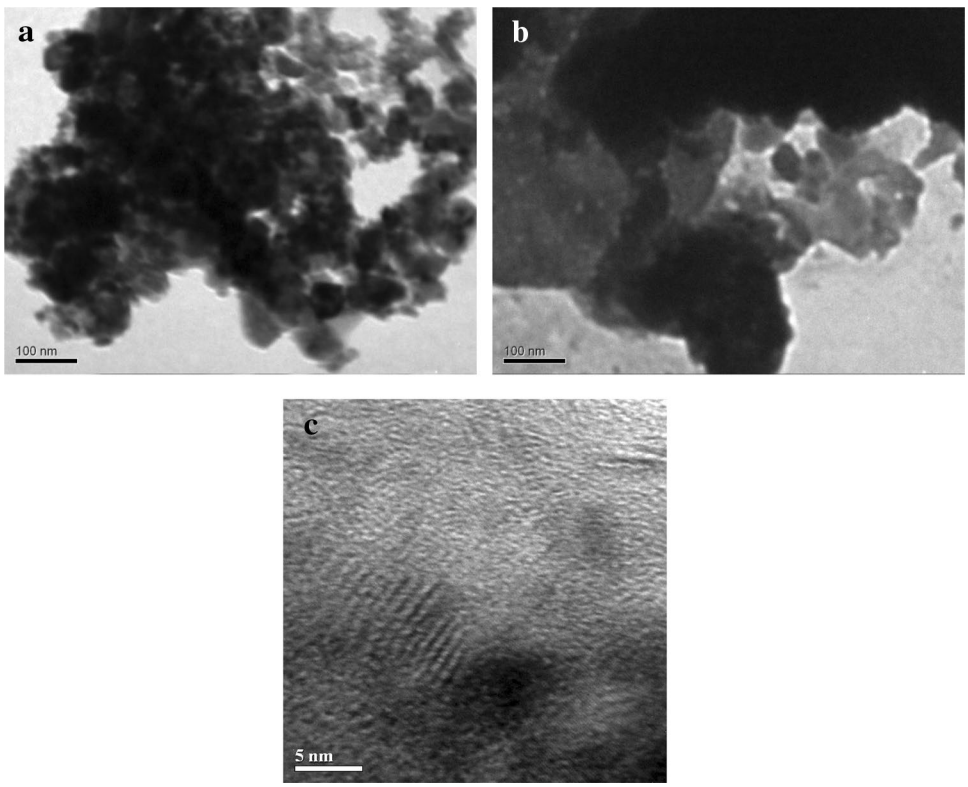

Fig. 3 Low-resolution TEM images of HZD-GO_{lm} (**a**) and ZHP-GO_{lm} (**b**), and high-resolution image of ZHP-GO_{lm} (**c**). The GO_{lm} content was 2%

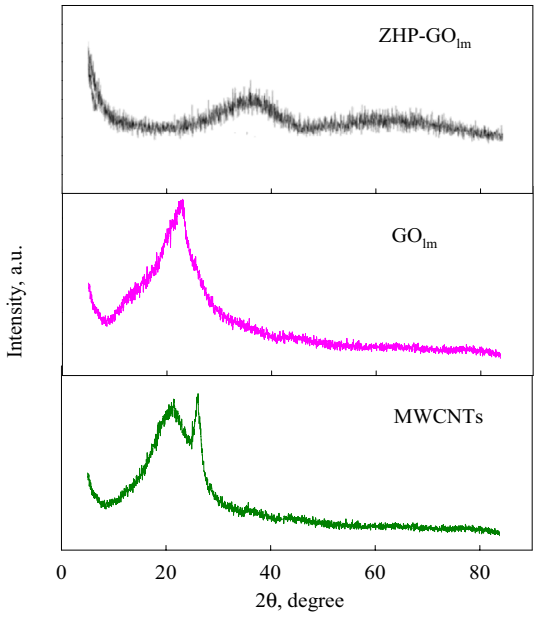

Fig. 4 XRD patterns for MWCNTs, GO_{lm}, and ZHP-GO_{lm}-containing 2% of the carbon material

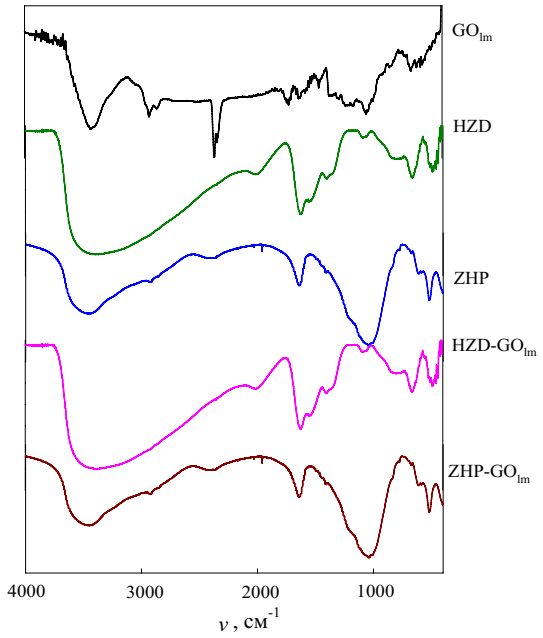

Fig. 5 FTIR spectra of GO_{lm}, inorganic matrices and composites containing 2% of GO_{lm}

present in the XRD pattern. However, the observed diffuse peak is located at larger angles; this indicates several walls of the carbon material obtained from MWCNTs.

The characteristic reflex for GO_{lm} is masked by inorganic matrix: the XRD pattern for the ZHP-GO_{lm} composite shows a wide galo, which is characteristic for amorphous materials. Similar results were obtained for the ZHP-GO_{lm} composite.

The data of FTIR spectroscopy are given in Fig. 5. The spectra for all samples show very broad peaks at 3400 cm^{-1}: these stripes are attributed to OH vibrations of water molecules. This peak is the widest for the inorganic ion exchangers and their composites. More narrow stripe is observed for the GO_{lm}.

The FTIR spectrum of GO_{lm} shows a number of peaks: they are attributed to stretching vibration of C–O–C (epoxy groups, 1070 cm^{-1}), C–OH (hydroxyl and carboxyl groups, 1257 cm^{-1}), O=C–OH (carboxyl groups, 1401 cm^{-1}), C–C (aromatics, i.e. carbon skeletal network, 1620 cm^{-1}), and C=O (carbonyl of carboxyl groups, 1722 cm^{-1}) (Zhao et al. 2015).

Characteristic peaks of HZD, which are attributed to metal–oxygen bonds, are as follows: stretching vibrations of Zr–O (Zr–OH surface groups, 490 cm^{-1}), Zr–O–Zr (bulk of particles, 550–750 cm^{-1}), Zr–OH (1380, 1553 cm^{-1}), and O–Zr–OH bonds (1640 cm^{-1}) (Kostrikin et al. 2010). Regarding ZHP, triply degenerates symmetric stretch vibration of PO_4 is at 1050 cm^{-1}. Addition of GO_{lm} causes no shift of the peaks related to metal–oxygen bonds. It means no chemical bonding graphene sheets with functional groups of inorganic matrices. Vibrations, which are related to GO_{lm}, are masked due to small amount of the carbon filler.

Porometric measurements

Isotherms of nitrogen adsorption–desorption are given in Fig. 6a, b. Regarding GO_{lm}, the isotherm is related to II type of IUPAC classification (Gregg and Sing 1982), since it is convex relatively abscissa axis in the region of low relative pressure (P/P_s) and concave at high pressure. The hysteresis loop is attributed rather to B type according to de Boer classification. This is characteristic for slit-like pores. At the same time, the isotherms for both inorganic sorbents and their composites are Langmuir type (type I) indicating microporous structure of the materials.

Differential pore-size distribution for GO_{lm} that were obtained according to the BJH method are plotted in Fig. 7. The narrow peak, which is related to smaller mesopores, indicates their ordering. Larger mesopores are disordered (the corresponding maximum is diffuse). Both HZD and its composite are practically non-porous within the interval of 10–100 nm. Considerable porosity has been found for lower r values. The maxima position is at $r < 1.5$ nm. The distributions for ZHP and ZHP-GO_{lm} samples look similarly.

The results of porometric measurements are summarized in Table 1. The value of specific surface area for GO_{lm} is much smaller than that calculated theoretically for isolated grapheme sheets (≈2600 m^2g^{-1}) as pointed in (Dreyer et al. 2010). This disagreement is due to

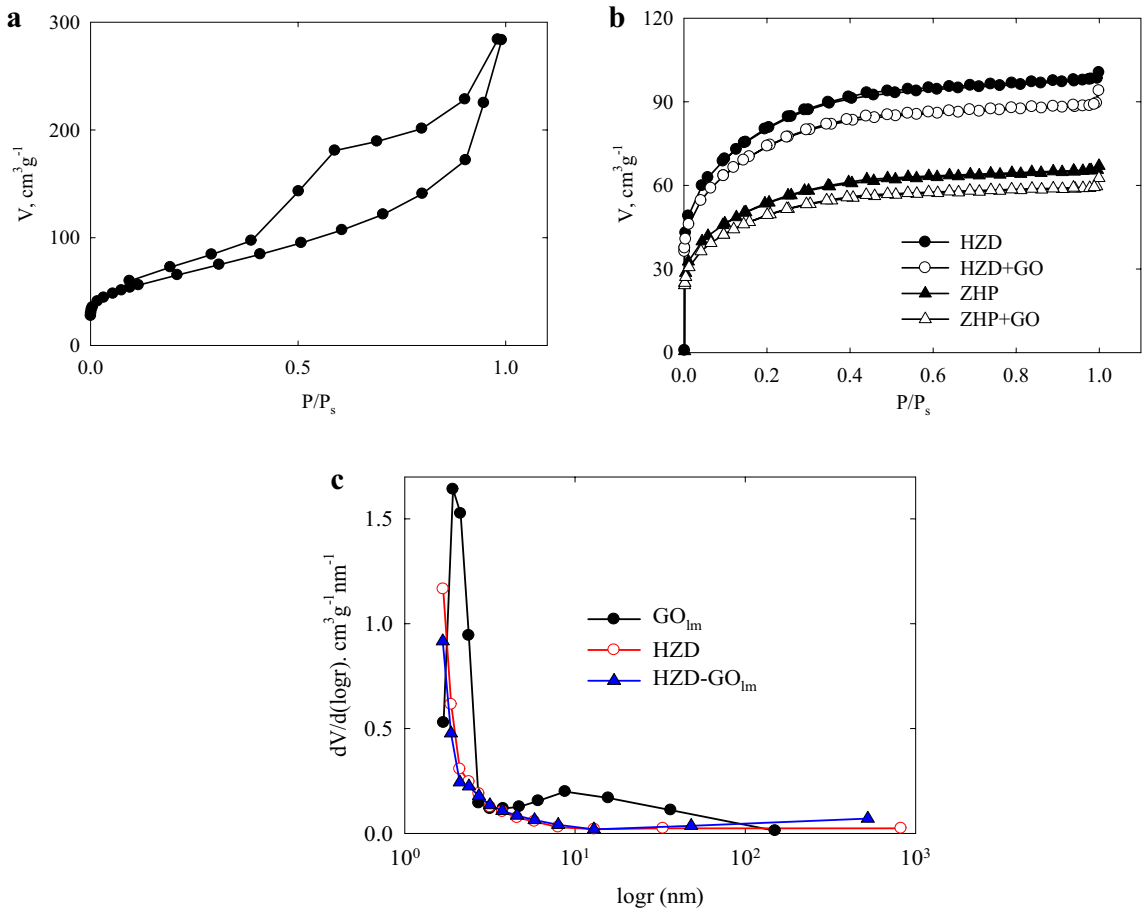

Fig. 6 Isotherms of adsorption–desorption of nitrogen for GO_{lm} (**a**), inorganic matrices and composites containing 2% of GO_{lm} (**b**), and differential pore-size distributions for some sorbents (**c**)

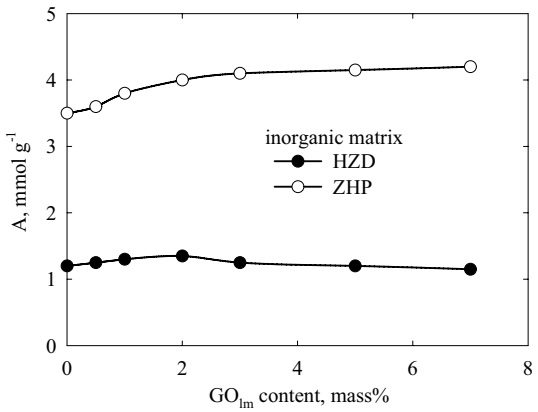

Fig. 7 Total adsorption capacity of composites towards K^+ ions as a function of GO_{lm} content

agglomeration, overlapping and curling the sheets of graphene. Nitrogen molecules cannot penetrate between the graphene sheets under low temperature. The values of surface area that are an order of magnitude higher were obtained for liquid adsorbates, such as water and octane.

Table 1 Pore structure and PZC of inorganic matrixes and their composites containing 2% of GO_{lm}

Sample	Volume, $cm^3\ g^{-1}$		Specific surface area, m^2g^{-1}	pH of PZC
	Micropores	Mesopores		
GO_{lm}	0.07	0.39	230	3.2
HZD	0.11	0.02	338	8.5
HZD-GO_{lm}	0.08	0.03	280	6.2
ZHP	0.06	0.02	165	2.0
ZHP- GO_{lm}	0.07	0.03	190	2.2

As opposed to ZHP, HZD is characterized by more developed surface comparing with GO_{lm} (Table 1). Lower value of surface area has been found for ZHP indicating coalescence of primary HZD particles during boiling in phosphoric acids. Indeed, this is confirmed by TEM images (see Figs. 2c, d) Additions of even small amount of GO_{lm} to HZD slightly reduce its microporosity and specific surface area.

At the same time, mesoporosity of the composite increases. When GO_{lm} is added to ZHP, the composite shows higher micro- and mesoporosity comparing with pure ZHP.

Acid base properties of composites and adsorption testing

Regarding GO, several mechanisms of the surface charge formation are known: (i) dissociation of carboxyl and phenolic groups, (ii) proton complexation of the π-electron system of graphene planes acting as Lewis basic sites, and (iii) protonation of Bronsted basic oxygen-containing fragments, such as epoxy- and carbonyl groups (Szabo et al. 2018). Dissociation causes cation-exchange ability of GO, protonation leads to anion adsorption. As found, dissociation dominates at pH > 3.2, while protonation occurs under lower pH (see Table 1). ZHP contains a several amount of −OH groups; they provide anion-exchange ability below pH 2. The composite containing higher basic GO_{lm} shows slightly higher pH of PZC. At last, GO_{lm} is more acidic than HZD. Thus, the addition of this carbon material causes a shift of the PZC to acidic region.

Increasing in GO_{lm} content in ZHP causes a growth of adsorption capacity towards K^+ ions (Fig. 7). This growth is rather rapid up to the amount of the carbon constituent of two mass %. The increase of capacity is 14% comparing with pure ZHP. This is due to highly developed surface of GO_{lm}. More loose structure of the composite provides the access for K^+ ions to adsorption sites, which are unavailable in pure ZHP. Moreover, GO_{lm} groups are also involved to ion exchange. Further increasing in GO_{lm} content causes no significant effect to adsorption: the growth of capacity is only 6%. This is due to a decrease of ZHP content. Namely $-OPO_3H_2$ groups provide high capacity, since they contain two counter-ions. As opposed to ZHP, the groups of GO_{lm} contain only one counter-ion. In general, the capacity of the composites is comparable with that for weakly acidic cation-exchange resins.

Carboxyl and phenolic groups of GO_{lm} provide a growth of adsorption capacity of the composites based on HZD. However, the samples containing more than 2% of GO_{lm} show a decrease of capacity probably due to compaction of the composites (specific surface area of GO_{lm} is lower comparing with pure HZD).

Thus, the optimal GO_{lm} content in the composites is 2%. Moreover, these materials form rather large granules (see Fig. 1a), a size of which is similar to the beads of ion-exchange resins. These composites were chosen for investigations of U(VI) adsorption.

U(VI) adsorption and desorption

Uranium (VI) exists in nitrate-containing solutions in a form of cationic complexes of UO_2^{2+}. Nevertheless, cationic species are sorbed by HZD in neutral media about PZC, since some −OH groups are dissociated under these conditions. Figure 8a illustrates the dependence of adsorption capacity over time (t). More than 50% of ions are removed from water in 4 h. Among known approaches, the model of pseudo-second order (Ho and McKay 1999) describes the experimental data most adequately. Following equation was applied:

$$\frac{t}{A} = \frac{1}{KA_\infty^2} + \frac{t}{A_\infty}, \tag{2}$$

where A_∞ is the capacity at $t \to \infty$, K is the rate constant. The data are given in Fig. 8b and Table 2.

As seen from Table 2, GO_{lm} depresses U(VI) adsorption on HZD. This is due to a decrease of the composite surface (lower A_∞ value) and bonding with carboxyl groups (slowdown of adsorption). At the same time, the A_∞ value

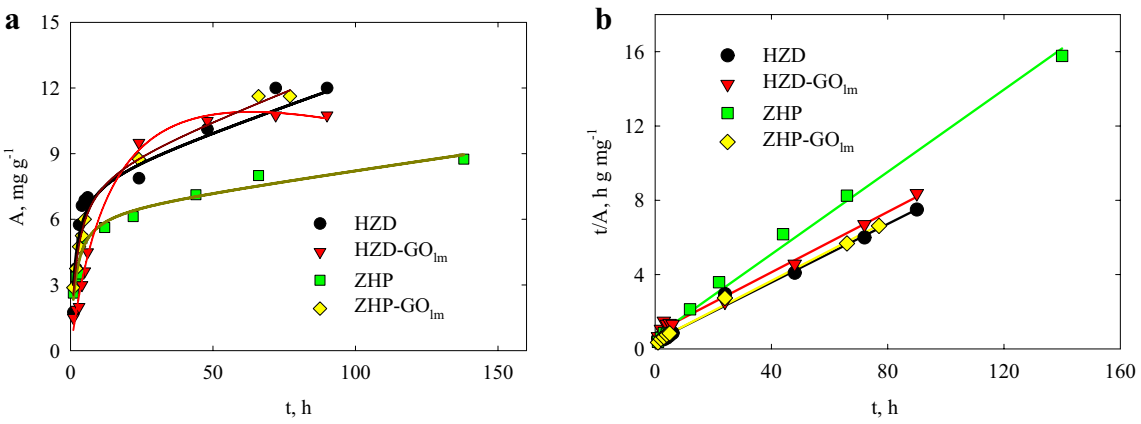

Fig. 8 Adsorption capacity of inorganic adsorbents and their composites, which contain 2% GO_{lm}, as a function of time (**a**) and these dependencies were simulated according to the model of pseudo-second order (**b**)

Table 2 Application of the models of pseudo-second order and DR to adsorption of U(VI) cations

Sample	Adsorption rate			Adsorption isotherm	
	A_∞, mg g^{-1}	K, g mg^{-1} h^{-1}	R^2	E, J mol^{-1}	R^2
HZD	12	1655	0.99	9601	0.98
HZD-GO$_{lm}$	11.4	1604	0.99	8133	0.98
ZHP	9.2	769	0.99	8810	0.98
ZHP- GO$_{lm}$	12.5	1929	0.99	13120	0.97

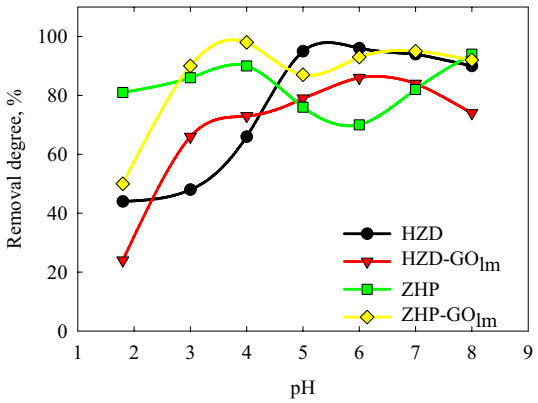

Fig. 9 Removal degree of U(VI) ions as a function of pH

for the ZHP-GO$_{lm}$ sample corresponds to maximal possible magnitudes, when the removal degree is 100%. The fastest adsorption has been found namely for this composite. Adsorption capacity A_∞, which has been found during investigations of adsorption rate, increases in the order: ZHP-GO$_{lm}$ > HZD > HZD-GO$_{lm}$ > ZHP. In general, GO$_{lm}$ improves sorption on ZHP only within a wide interval of pH (2–7), where dissociation of carboxyl groups occurs (Fig. 9).

High removal degree is achieved despite significant excess of hardness ions. In the case of HZD-GO$_{lm}$, it demonstrates higher removal degree than pure HZD only at pH 2, 5–4.

Isotherms of UO_2^{2+} adsorption are given in Fig. 10a. For the equilibrium conditions, the adsorption capacity increases in the order: ZHP-GO$_{lm}$ > HZD > ZHP > HZD-GO$_{lm}$. The Langmuir, BET, Freundlich, and Dubinin–Radushkevich (DR) models (Rieman and Walton 1970) were applied to the isotherms. As found, the most suitable is the DR model (Fig. 10b):

$$\ln A = \ln A_{DR} - \frac{R^2T^2}{E^2}[\ln(1 + 1/c)]^2, \quad (3)$$

which has been found to give linear approximation within a certain interval of concentration of equilibrium solution. Here, A_{DR} is the constant and E is the adsorption energy. The DR model corresponds to full filling of micropores with large UO_2^{2+} ions. The energy values are in the interval of 8–16 kJ mol^{-1} indicating ion-exchange mechanism. However, the data of sorption kinetics show an additional interaction with functional groups. This is typical for inorganic matrices and their composites. Regarding nitrate solutions, the pH of which is 7, U(VI) is in a form of the mixture of neutral ($(UO_2)(OH)_2$) and cationic ($((UO_2)_3(OH)_5^+$, $(UO_2)_4(OH)_7^+$) hydroxocomplexes (Cornelis et al. 2005). It is possible to suppose that the interaction of uranyl complexes with the functional groups of the adsorbent is due to surface complexation. This is evidently more characteristic for the composite based on ZHP, since the maximal uranyl uptake and the highest adsorption energy. However, this assumption requires confirmations in a future. The best kinetic characteristics of the ZHP-GO$_{lm}$ sample could be explained by a decrease of the micropore volume and increase of mesoporosity. Increase of pore size accelerates ion transport (Volfkovich 1984; Volfkovich et al. 1999).

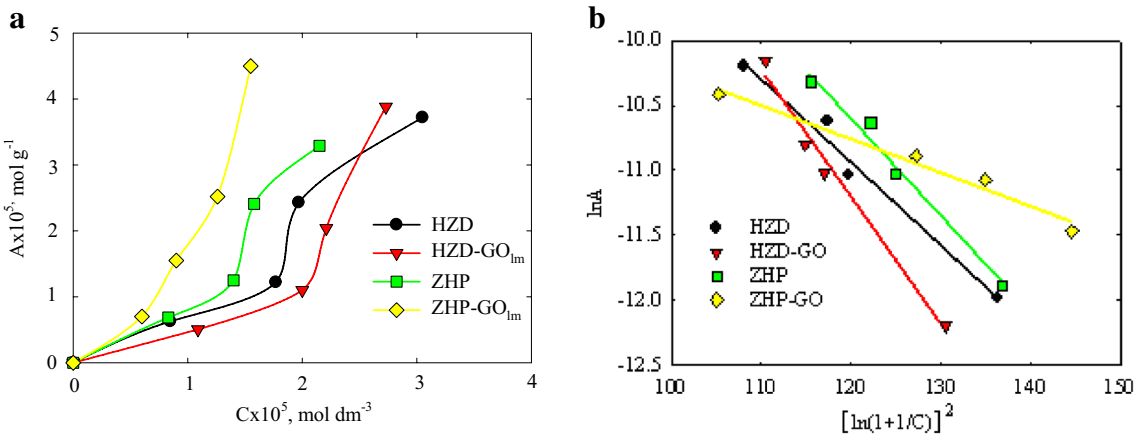

Fig. 10 Isotherms of U(VI) sorption: initial data (**a**) and application of DR model (**b**)

Table 3 Regeneration of sorbents

Sample	Regeneration degree, %		
	H_2O	HNO_3	$NaHCO_3$
HZD	5	70	78
HZD-GO_{lm}	3	65	55
ZHP	3	80	98
ZHP- GO_{lm}	2	92	70

The indirect confirmation of chemosorption is the data obtained during regeneration of U(VI) loaded adsorbents with deionized water (Table 3). As follows from the table, the desorption degree is very low indicating a significant contribution of chemosorption to the adsorption mechanism. As found, GO_{lm} deteriorates regeneration of the HZD-based composite comparing with pure HZD (Table 3). In the case of ZHP, regeneration with sodium hydrocarbonate is preferable. The highest regeneration degree of the ZHP-GO_{lm} sample is achieved when the solution of nitric acid is used. The development of regeneration conditions is the task of further investigations.

Concluding remarks

GO_{lm}, which was obtained by treatment of MWCNTs, can be considered as an addition to sorbents for U(VI) removal. Comparing with the traditional GO synthesis techniques, the method of MWCNTs' disclosure is more eco-friendly. This carbon material increases the specific surface area of ZHP and reduces it in the case of HZD. Comparing with pure inorganic materials, sorption of U(VI) cations is improved on the ZHP-based composite and deteriorated on the sorbent based on HZD. The mechanism of sorption is ion exchange, which is accompanied by an additional interaction of sorbed ions with functional groups. The composite based on ZHP shows also high regeneration degree in the solution of nitric acid.

Increasing in GO_{lm} content in composites causes a decrease of their granules evidently due to screening of aggregates of primary particles with graphene sheets. The optimal content of the carbon addition is 2%, which provides the formation of large granules. Considerable removal degree of U(VI) is achieved even in the presence of significant excess of hardness ions. Thus, this material can be used as a filler of sorption columns. Higher sorption capacity towards U(VI) is possible under higher content of GO_{lm}. In this case, the sorbents should be fixed in a support. The composites are expected to be effective towards other toxic cations.

Acknowledgements The work was performed within the framework of the projects entitled "Developments of materials and processes for removal of valuable and toxic components from the solutions of biogenic and technogenic origin" (supported by the NAS of Ukraine).

Compliance with ethical standards

Conflict of interest On behalf of all authors, the corresponding author states that there is no conflict of interest.

References

Ali AH (2018) Potentiality of zirconium phosphate synthesized from zircon mineral for uptaking uranium. Separ Sci Technol 53(14):2284–2296

Alirezazadeh N, Garshasbi H (2003) A survey of natural uranium concentrations in drinking water supplies in Iran. Iran J Radiat Res 1(3):139–142

Almazan-Torres MA, Drot P, Mercier-Bion F, Catalette H, Auwer CD, Simoni E (2008) Surface complexation modeling of uranium(VI) sorbed onto zirconium oxophosphate versus temperature: Thermodynamic and structural approaches. J Colloid Interface Sci 323(1):42–51

Amphlett CB (1964) Inorganic ion exchangers. Elsevier, Amsterdam

Awwad NS (2018) Uranium: safety, resources, separation and thermodynamic calculation. IntechOpen, London

Bachmaf S, Merkel BJ (2011) Sorption of uranium(VI) at the clay mineral–water interface. Environ Earth Sci 63:925–934

Brine W (2010) The toxicity of depleted uranium. Int J Environ Res Public Health 7:303–313

Cornelis R, Caruso JA, Crews H, Heumann KG (2005) Handbook of elemental speciation II. Species in the environment, food, medicine and occupational health, Wiley, Chichester

Criscenti LJ, Sverjensky DA (1999) The role of electrolyte anions (ClO_4^-, NO_3^-, and Cl^-) in divalent metal (M^{2+}) adsorption on oxide and hydroxide surfaces in salt solutions. Environ Sci 31(17):828–899

Danilov MO, Slobodyanyuk IA, Rusetskii IA, Kolbasov GY (2016a) Synthesis of reduced graphene oxide obtained from multiwalled carbon nanotubes and its electrocatalytic properties. In: Aliofkhazraei M, Ali N, William I. Milne WI, Ozkan CS, Mitura S, Gervasoni JL (eds) Graphene science handbook: fabrication methods. CRS press, Boca Raton, London, New York, pp 205–226

Danilov MO, Rusetskii IA, Slobodyanyuk IA, Dovbeshko GI, Kolbasov GY, Strubov YY (2016) Synthesis, properties, and application of graphene-based materials obtained from carbon nanotubes and acetylene black. Ukr J Phys 7(1):3–11

Dragan ES, Avram E, Axente D, Marcu C (2004) Ion-exchange resins. III. Functionalization–morphology correlations in the synthesis of some macroporous, strong basic anion exchangers and uranium-sorption properties evaluation. J Polym Sci 42(10):2451–2461

Dreyer DR, Park S, Bielawski CW, Ruoff RS (2010) The chemistry of grapheme oxide. Chem Soc Rev 39(1):228–240

Drot R, Simoni E, Alnot M, Ehrhardt JJ (1998) Structural environment of uranium (VI) and europium (III) species sorbed onto phosphate surfaces: XPS and optical spectroscopy studies. J Interface Colloid Sci 205(2):410–416

Dzyazko YS, Perlova OV, Perlova NA, Volfkovich YM, Sosenkin VE, Trachevskii VV, Sazonova VF, Palchik AV (2017) Composite cation-exchange resins containing zirconium hydrophosphate for purification of water from U(VI) cations. Desalin Water Treat 69:142–152

Dzyazko YS, Trachevskii VV, Rozhdestvenskaya LM, Vasilyuk SL, Belyakov VN (2013) Interaction of sorbed Ni (II) ions with amorphous zirconium hydrogen phosphate. Russ J Phys Chem 87(5):840–845

Dzyazko YS, Ogenko VM, Volfkovich YM, Sosenkin VE, Maltseva TV, Yatsenko TV, Kudelko KO (2018) Composite consisting of hydrated zirconium dioxide and grapheme oxide for removal of organic and inorganic components from water. Chem Phys Technol Surf 9(4):417–431

Dzyazko YS, Volfkovich YM, Sosenkin VE, Nikolskaya NF, Gomza YP (2014) Composite inorganic membranes containing nanoparticles of hydrated zirconium dioxide for electrodialytic separation. Nanoscale Res Let 9(1):271. https://doi.org/10.1186/1556-276X-9-27

Dzyazko Y, Kolomyets E, Borysenko Y, Chmilenko V, Fedina I (2019) Organic-inorganic sorbents containing hydrated zirconium dioxide for removal of chromate anions from diluted solutions. Mater Today Proc 6(2):260–269

Dzyaz'ko YS, Belyakov VN, Stefanyak NV, Vasilyuk SL (2006) Anion-exchange properties of composite ceramic membranes containing hydrated zirconium dioxide. Russ J Appl Chem 79(5):769–773

Everett J (1998) Adsorption of Metals by Geomedia: Variables, Mechanisms, and Model Applications. Academic Press, San-Diego, London, Boston, New York, Sidney, Tokyo, Toronto

Gilson ER, Huang S, Jaffé PR (2015) Biological reduction of uranium coupled with oxidation of ammonium by *Acidimicrobiaceae* bacterium A6 under iron reducing conditions. Biodegradation 26(6):475–482

Futaba DN, Yamada T, Kobashi K, Yumura M, Hata K (2011) Macroscopic wall number analysis of single-walled, double-walled, and few-walled carbon nanotubes by X-ray diffraction. J Am Chem Soc 133(15):5716–5719

Gregg SJ, Sing KSW (1982) Adsorption, Surface Area and Porosity. Academic Press, London

Gönder ZB, KayaI Y, Vergili I, Barlas H (2006) Capacity loss in an organically fouled anion exchanger. Desalination 189(1–3):303–307

Gu B, Ku Y-K, Jardine PM (2004) Sorption and binary exchange of nitrate, sulfate, and uranium on an anion-exchange resin. Environ Sci Technol 38(11):3184–3188

Ho YS, McKay G (1999) Pseudo-second order model for sorption processes. Process Biochem 34:451–465

Hoover J, Gonzales M, Shuey C, Barney Y, Lewis J (2017) Elevated arsenic and uranium concentrations in unregulated water sources on the navajo nation, USA. Exposure and Health 9(2):113–124

Kadam BV, Maiti B, Sathe RM (1981) Selective spectrophotometric method for the determination of uranium(VI). Analyst 106(1263):724–726

Kao D-Y, Chen L-C, Wen T-J, Chu C-F (2016) Study on the leachable behavior of cation exchange resins. J Nucl Sci Technol 53(6):921–927

Khawassek YM, Masoud AM, Taha MH, Hussein AEM (2018) J Radioanal Nucl Chem 315(3):493–502

Kostrikin AV, Spiridonov FM, Komissarova LN, Lin'ko IV, Kosenkova OV (2010) On the structure and dehydration of hydrous zirconia and hafnia xerogels. Russ J Inorg Chem 55(6):866–875

Leybros A, Roubaud A, Guichardon P, Boutin O (2010) Ion exchange resins destruction in a stirred supercritical water oxidation reactor. J Supercrit Fluids 51(3):369–375

Ling L, Zhang W-x (2015) Enrichment and encapsulation of uranium with iron nanoparticle. J Am Chem Soc 137(8):2788–2791

Liu W, Zhao X, Wang T, Zhao D, Ni J (2016) Adsorption of U(VI) by multilayer titanate nanotubes: effects of inorganic cations, carbonate and natural organic matter. Chem Eng J 286:427–435

Liu X, Du P, Pan W, Dang C, Qian T, Liu H, Liu W, Zhao D (2018) Immobilization of uranium(VI) by niobate/titanate nanoflakes heterojunction through combined adsorption and solar-light-driven photocatalytic reduction. Appl Catal B: Environ 231:11–22

Loon LR, Hummel W (1999) The degradation of strong basic anion exchange resins and mixed-bed ion-exchange resins: effect of degradation products on radionuclide speciation. Nucl Technol 128(3):388–401

Luo X, Wang C, Wang L, Deng F, Luo S, Tu X, Au C (2013) Nanocomposites of graphene oxide-hydrated zirconium oxide for simultaneous removal of As(III) and As(V) from water. Chem Eng J 220:98–106

Metilda P, Sanghamitra K, Gladis JM, Naidu GRK, Prasada Rao T (2005) Amberlite XAD-4 functionalized with succinic acid for the solid phase extractive preconcentration and separation of uranium(VI). Talanta 65(1):192–200

Ordoñez-Regil E, Drot R, Simoni E (2003) Surface complexation modeling of uranium(VI) sorbed onto lanthanum monophosphate. J Colloid Interface Sci 263(2):391–399

Orloff KG, Mistry K, Charp P, Metcalf S, Marino R, Shelly T, Melaro E, Donohoe AM, Jones RL (2004) Human exposure to uranium in groundwater. Environ Res 90(3):319–326

Outokesh M, Sepehrian H, Kosari M, Fasihi J (2016) Uranium ions removal using Amberlite CG-400 anion exchanger resin in the presence of sulfate anions. Int J Eng 29(6):728–734

Pan Z, Li W, Fortner JD, Giammar DE (2017) Measurement and surface complexation modeling of U(VI) adsorption to engineered iron oxide nanoparticles. Environ Sci Technol 51(16):9219–9226

Perlova OV, Tekmenzi KI, Perlova NA, Polikarpov AP (2019) Fibrous ion-exchangers FIBAN as sorbents of uranium(VI) compounds present in sulfate solutions. Odesa Natl Univ Herald Chem 24(3):75–89 **in Ukrainian**

Perlova N, Dzyazko Y, Perlova O, Palchik A, Sazonova V (2017) Formation of zirconium hydrophosphate nanoparticles and their effect on sorption of uranyl cations. Nanoscale Res Lett 12:209. https://doi.org/10.1186/s11671-017-1987-y

Perlova O, Dzyazko Y, Halutska I, Perlova N, Palchik A (2018) Anion exchange resin modified with nanoparticles of hydrated zirconium dioxide for sorption of soluble U(VI) compounds. Springer Proc Phys 210:3–15

Pourbeyram S (2016) Effective removal of heavy metals from aqueous solutions by graphene oxide–zirconium phosphate (GO–Zr–P) nanocomposite. Ind Eng Chem Res 55(19):5608–5617

Reinoso-Maset E, Ly J (2016) Study of uranium(VI) and radium(II) sorption at trace level on kaolinite using a multisite ion exchange model. J Environ Radioact 157:136–148

Rieman W, Walton H (1970) Ion exchange in analytical chemistry. Pergamon Press, Oxford, New York, Toronto, Sydney, Braunschweig

Sazonova VF, Perlova OV, Perlova NA, Polikarpov AP (2017) Sorption of uranium (VI) compounds on fibrous anion exchanger surface from aqueous solutions. Colloid J 79(2):270–277

Seredych M, Bandosz TJ (2011) Reactive adsorption of hydrogen sulfide on graphite oxide/$Zr(OH)_4$ composites. Chem Eng J 166:1032–1038

Seredych M, Bandosz TJ (2010) Effects of surface features on adsorption of SO_2 on graphite oxide/$Zr(OH)_4$ composites. J Phys Chem 114(34):14552–14560

Somasekhara Reddy MC, Sivaramakrishna L, Varada Reddy A (2012) The use of an agricultural waste material Jujuba seeds for the removal of anionic dye (Congo red) from aqueous medium. J Hazard Mater 203–204:118–127

Szabo T, Tombacz E, Illes E, Dekany I (2018) Enhanced acidity and pH-dependent surface charge characterization of successively oxidized graphite oxides. Carbon 44:537–545

Tan L, Wang Y, Liu Q, Wang J, Jing X, Liu L, Liu J, Song D (2015) Enhanced adsorption of uranium (VI) using a three-dimensional layered double hydroxide/graphene hybrid material. Chem Eng J 259:752–760

Um W, Serne RJ, Brown CF, Rod KA (2008) Uranium(VI) sorption on iron oxides in hanford site sediment: application of a surface complexation model. Appl Geochem 23(9):2649–2657

Volfkovich YM, Rychagov AY, Sosenkin VE, Efimov ON, Os'makov MI (2014) Measuring the specific surface area of carbon nanomaterials by different methods. Russ J Electrochem 50(11):1099–1101

Volfkovich YM, Sergeeva AG, Zolotova TK, Afanasieva SD, Efimov ON, Krinichnaya EP (1999) Macrokinetics of polyaniline based electrode: effects of porous structure, microkinetics, diffusion, and electrical double layer. Electrochim Acta 44(10):1543–1558

Volfkovich YM (1984) Influence of the electric double-layer on the internal interfaces in an ion-exchanger on its electrochemical and sorption properties. Soviet Electrochem 20(5):621–628

Wang F, Liu Q, Li R, Li Z, Zhang H, Liu L, Wang J (2016) Selective adsorption of uranium(VI) onto prismatic sulfides from aqueous solution. Colloids Surfaces A: Physicochem Eng Aspects 490:215–221

Wen Z, Huang K, Niu Y, Yao Y, Wang S, Cao Z, Zhong H (2019) Kinetic study of ultrasonic-assisted uranium adsorption by anion exchange resin. Physicochem Eng Aspects Coll Surf A. https://doi.org/10.1016/j.colsurfa.2019.124021

Yang A, Zhu Y, Huang CP (2018) Facile preparation and adsorption performance of graphene oxide-manganese oxide composite for uranium. Sci Rep 8:90584. https://doi.org/10.1038/s41598-018-27111-y

Zakutevskyy OI, Psareva TS, Strelko VV (2012) Sorption of U(VI) ions on sol-gel-synthesized amorphous spherically granulated titanium phosphates. Russ J Appl Chem 85(9):1366–1370

Zhao J, Liu L, Li F (2015) Graphene oxide: physics and applications. Springer, Heidelberg, New York, Dordrecht, London

Zvezdov A, Ishigure K (2003) The effect of corrosion particles present in water solutions on the behavior of strong acid cation-exchange resins during the process of cobalt removal. Desalination 154(2):153–160